Niobate Nanosheets as Catalysts for Photochemical Water Splitting into Hydrogen and Hydrogen Peroxide

Owen C. Compton and Frank E. Osterloh*

Department of Chemistry, University of California—Davis, One Shields Avenue, Davis, California 95616

Received: September 3, 2008; Revised Manuscript Received: October 26, 2008

Tetrabutylammonium-stabilized $Ca_2Nb_3O_{10}$ nanosheets catalyze photochemical splitting of water into hydrogen and hydrogen peroxide under UV irradiation. The peroxide forms on the surface of the catalyst and adsorbs to it, fully deactivating the catalyst after 48 h of irradiation. For the Pt-modified niobate, complete deactivation occurs within 24 h due to higher H_2 evolution rate with this system. The peroxide was identified via Raman and IR spectroscopy. In vibrational spectra, the irradiated niobate exhibits bands at 580, 778, and 940 cm^{-1}, which suggest that the peroxide is present as a side-on ligand coordinated to the Nb^{5+} ions on the nanosheet surface. The same species can be formed by treating the nanosheets with 30% aqueous H_2O_2. If the catalyst is irradiated in $H_2{}^{18}O$, the bands shift to lower energy, indicating that the peroxide species is formed from water. Room-temperature storage of the nanosheets in $H_2{}^{18}O$ also leads to isotopic exchange of all Nb−O atoms over the course of 24 h. Peroxide amounts measured by titration of the catalyst with *o*-tolidine after 6, 12, and 24 h of irradiation form in a 1:1 stoichiometry with hydrogen. Infrared data shows that the peroxide is partially desorbed by evacuating the catalyst and by purging with argon gas. Under catalytic conditions, this treatment restores up to 60% of the original activity. For the H_2O_2-treated catalyst, near quantitative H_2O_2 desorption occurs within 20 min at 450 °C. Separate irradiation experiments of the catalyst in the presence of air reveal that H_2 evolution is diminished and that O_2 uptake occurs from the atmosphere. Most of the hydrogen peroxide formed under these conditions is subsequently detected in the supernatant and only small amounts on the catalyst. NMR spectra show that the tetrabutylammonium cations are decomposed. These findings suggest that there are two distinct pathways for peroxide formation, one involving one-electron reduction of O_2 and one involving two-electron reduction of water (in the absence of O_2).

Introduction

Since the discovery of photooxidation of water with TiO_2 (rutile) by Fujishima and Honda in 1971,[1,2] the photocatalytic water splitting reaction (eq 1) has been widely investigated as a possible process for generating fuel.[3−5] Catalysts for this reaction typically consist of a compound semiconductor and a fused metal or metal oxide cocatalyst. If the band gap of the material is large enough (at least 2.4 eV),[6,7] irradiation of an aqueous catalyst dispersion can lead to H_2 and O_2. However, for many metal oxides, including the anatase form of TiO_2,[8−11] several titanates, and niobates ($KCa_2Nb_3O_{10}$,[12] $Sr_2Nb_6O_7$,[13] and $K_4Nb_6O_{17}$[14]), O_2 evolution is often substoichiometric or no O_2 is observed at all, even though the band gaps of these semiconductors are suitable for overall splitting of water. Grätzel and later Arakawa's group[15−17] have investigated this phenomenon in greater detail. For anatase powders with or without Rh- or Pt-cocatalysts, it was found that no O_2 is evolved and that H_2 evolution ceases after 28 h.[9−11,18−20] Using a redox active dye it was shown that peroxide/superoxide species were produced during the reaction (eq 2), and that these species adsorbed to the catalyst surface and deactivated it over time. However, the binding geometry of the peroxides could not be determined. Also it was not clear if the peroxide formed by two-electron oxidation of water as shown in eq 6, or by four-electron oxidation of water (eq 1), followed by two-electron reduction of O_2 (eq 3).

$$H_2O \xrightarrow{h\nu,\ \text{cat}} H_2 + {}^1\!/_2O_2 \quad (1)$$

$$2H_2O \xrightarrow{h\nu,\ \text{cat}} H_2 + H_2O_{2(\text{ads})} \quad (2)$$

$$2H^+ + 2e_{CB}{}^- + O_2 \xrightarrow{h\nu,\ \text{cat}} H_2O_{2(\text{ads})} \quad (3)$$

$$e_{CB}{}^- + O_2 \xrightarrow{h\nu,\ \text{cat}} O_2{}^{\bullet -} \quad (4)$$

$$2H^+ + e_{CB}{}^- + O_2{}^{\bullet -} \xrightarrow{h\nu,\ \text{cat}} H_2O_{2(\text{ads})} \quad (5)$$

$$2H_2O + 2h_{VB}{}^+ \xrightarrow{h\nu,\ \text{cat}} H_2O_{2(\text{ads})} + 2H^+ \quad (6)$$

$$RH + H^+ + O_2{}^{\bullet -} \rightarrow H_2O_2 + R^{\bullet} \quad (7)$$

$$H_2O_2 \rightarrow {}^1\!/_2O_2 + H_2O \qquad \Delta G = -98.0\ \text{kJ mol}^{-1} \quad (8)$$

Reaction 3 is known to be a source for H_2O_2 when TiO_2 is irradiated in the presence of O_2. On anatase, the main oxygen reduction product is hydrogen peroxide, whereas on rutile the main product is superoxide ion.[21] Graetzel speculated that on anatase reaction 3 proceeds in two one-electron steps with free superoxide radicals as intermediates (eqs 4/5).[9] Using electrochemical data, Augustinsky could show that for anatase TiO_2 (but not for rutile) two-electron oxidation of water (eq 6) does

* To whom correspondence should be addressed.

10.1021/jp807839b CCC: $40.75
Published on Web 12/12/2008

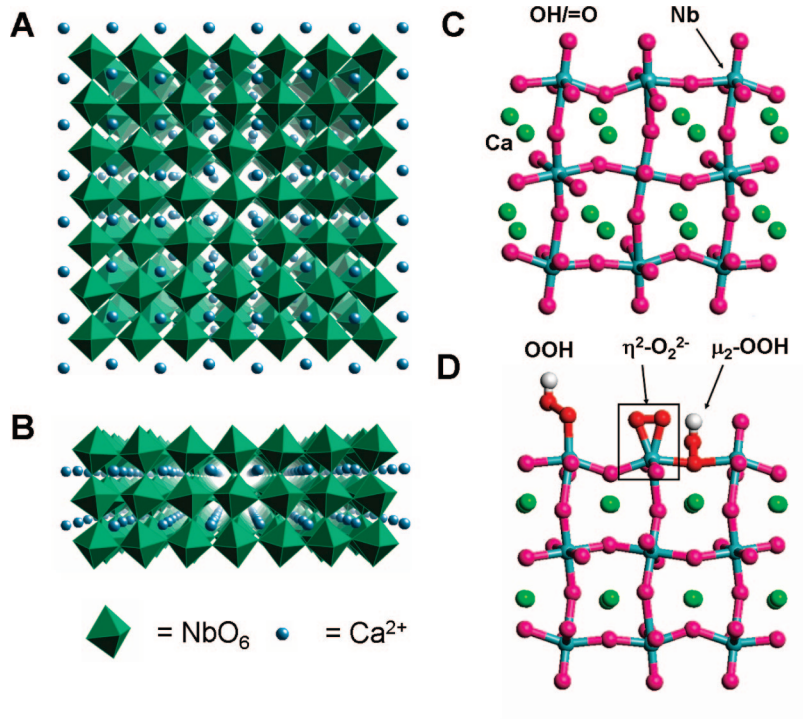

Figure 1. Crystallographic structure of a single TBA[$Ca_2Nb_3O_{10}$] nanosheet viewed (A) along and (B) perpendicular to the surface normal. (C) Ball and stick model of a layer fragment (side view). The nanosheet surfaces are terminated by Nb═O and Nb−O^- groups that can interact with the surrounding water. (D) Possible coordination modes of peroxide to nanosheet surface. The framed coordination mode is observed.

occur.[22,23] He suggested that the peroxide would bind either as side-on η^2-ligand or as terminal HOO− ligand to a Ti surface ion, or as $\mu_2-\eta^2$-ligand bridging between two adjacent Ti surface sites.

Here we describe our results of an investigation of the mechanism of photochemical water conversion using nanosheets derived from the known photochemical catalyst $KCa_2Nb_3O_{10}$ ($E_G = 3.3-3.5$ eV).[5,12,24−28] As we reported before, dispersions of individual nanosheets are able to evolve H_2 from water under UV light, but no oxygen.[29−31] We now find that hydrogen evolution with the niobate sheets is coupled with stoichiometric formation of peroxide, according to eq 2. This peroxide does not form via reduction of O_2 (eq 3), since irradiation experiments conducted in the presence of O_2 mostly lead to free H_2O_2 and only to small amounts of coordinated peroxide. According to vibrational spectra, the peroxide is present as side-on bound ligand on the surface-Nb sites (Figure 1D). Our findings are important because they shed further light on the inability of certain catalysts to cleave water into H_2 and O_2, and because they confirm reaction 2 as a water splitting pathway that leads to H_2O_2 and H_2. Hydrogen peroxide generated in this way could be of potential value as a fuel according to eq 8.

Experimental Section

Materials. *o*-Tolidine (95%) was obtained from Acros Organics and was purified according to literature procedures.[32] $H_2{}^{18}O$ water (>98%) was received from Medical Isotopes, Incorporated. Methanol was received from Fisher Scientific. All water used was purified by a Nanopure II system to a resistivity of >18 MΩ cm.

TBA[$Ca_2Nb_3O_{10}$] Synthesis. The Dion−Jacobsen phase $HCa_2Nb_3O_{10}$ was synthesized according to literature procedures.[33] This product was delaminated by treatment with a 20 mol excess of TBA(OH), resulting in individually dispersed TBA[$Ca_2Nb_3O_{10}$] nanosheets.[34] Exfoliated nanosheets were stored in aqueous solution at pH = 11 to discourage restacking. Solution concentrations were 0.15 M for nanosheets and 1.0 M for TBA(OH). Aliquots containing 100 mg of nanosheets were diluted to 50 mL with water before catalytic measurements.

Pt-TBA[$Ca_2Nb_3O_{10}$] Synthesis. Platinum nanoparticles were grown on the surface of TBA[$Ca_2Nb_3O_{10}$] by photodeposition as described earlier.[27] Samples in this study contained 3 wt % of the platinum cocatalyst, as in previous preparations.[29,31] The product, Pt-TBA[$Ca_2Nb_3O_{10}$], was collected by centrifugation and washed twice with 50 mL aliquots of water.

Reaction with H_2O_2. A 25 mg sample of TBA[$Ca_2Nb_3O_{10}$] was diluted to 10 mL in a 0.2 M solution of H_2O_2. The solution was shaken and left overnight before collection of the precipitate, which began to form after 3 h.

Irradiation and H_2/O_2 Measurement. Solutions of catalysts were irradiated simultaneously with four 175 W low-pressure mercury lamps that delivered a combined quantum flux of 5.82×10^{-7} mol/s inside the test flask as measured by ferrioxalate actinometry.[35] Quantum efficiencies were calculated (QE = $2 \cdot [H_2]/I$) from the quantum flux of the irradiation system (I) and the average rate of H_2 evolution in moles per second. A 100 mL quartz flask, directly connected to a gas chromatograph via a gas valve, was filled with 50 mL of aqueous solution containing 100 mg of catalyst. The flask was evacuated and purged three times with argon gas to remove any dissolved gases in the solution. The flask was irradiated while stirring, and samples were periodically withdrawn directly from the flask into a gas chromatograph. For O_2 adsorption measurements, 2 mL of O_2 gas was injected into the atmosphere above the flask through a rubber septum using a gas-tight syringe.

Assay with *o*-Tolidine. Hydrogen peroxide measurements were performed on 2.0 mL aliquots of the catalyst suspension that were removed after varying periods of irradiation. For each test, a 0.5 mL volume of 1% *o*-tolidine in 0.1 M HCl was added to the suspension along with 1.0 mL of colloidal platinum

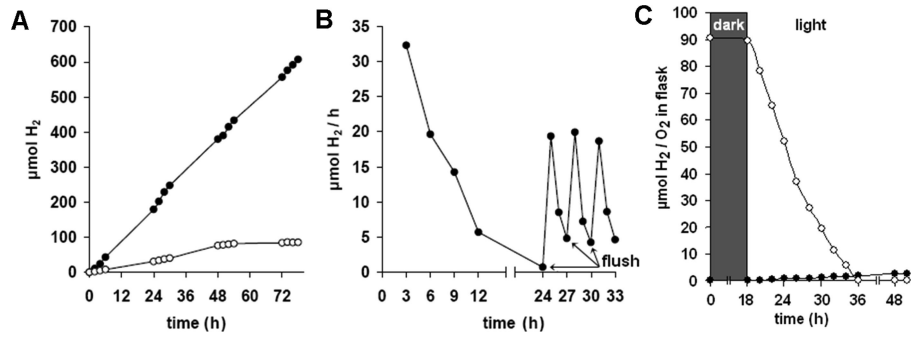

Figure 2. (A) H_2 evolution data for water (○) and 20% aqueous methanol (●) using 100 mg nanosheets. (B) Rate of H_2 evolution from Pt-$[HCa_2Nb_3O_{10}]$ as a function of time. Arrows indicate evacuation to 20 torr followed by purging with Ar gas. (C) Evolution of H_2 (●) and of added O_2 (○) under irradiation.

prepared as explained previously.[29] This mixture was allowed to react for 5 min. A blue color indicative of oxidized *o*-tolidine evolved within 30 s. A volume of 0.5 mL of 1 M HCl was then added, generating a yellow color. The product was centrifuged, and the supernatant was removed and diluted to 10 mL with water. The absorbance of the solution was then measured with a UV−vis spectrophotometer. The instability of the product at room temperature (complete decomposition after ~1 h) required consistent reaction periods for quantitative measurement. Solutions of nonirradiated TBA$[Ca_2Nb_3O_{10}]$ did not turn blue after addition of *o*-tolidine and were faintly yellow after addition of HCl. A calibration curve was obtained by reacting solutions of H_2O_2, ranging in concentration from 8.8×10^{-5} to 1.3×10^{-3} M, in place of the nanosheet sample, yielding an extinction coefficient of 932 $M^{-1} \cdot cm^{-1}$, which compares well to previously determined values.[18,20]

IR and Raman Sample Preparation. Samples of nanosheets were centrifuged from solution, and the precipitates were collected. Thin layers of precipitate were dried on a KBr plate for IR measurements, or a glass slide for Raman measurements, and promptly analyzed.

NMR Sample Preparation. Samples of irradiated nanosheets were dried under vacuum. Dried residues were dissolved in D_2O. Samples were added to an NMR tube, taking care to not include any solids.

Instrumentation. Gas samples from the reaction space above the irradiated solutions were injected into a gas chromatograph employing Ar as the carrier gas. Sample components were separated with a Supelco molecular 60/80 sieve 5 Å column and detected with a thermal conductivity detector (TCD). UV/vis spectra were collected using an Ocean Optics DH2000 light source and HR2000 CG-UV−NIR spectrometer. Infrared spectra were collected with a Tensor 27 FT-IR spectrometer from Bruker Optics. Raman spectra were collected using a Renishaw RM1000 microspectrometer. A Fisher Scientific Marathon 21000 centrifuge at 13 750 rpm was employed for centrifugation. H^1-NMR spectra were obtained with either a Varian Inova 400 MHz or Bruker Avance 600 MHz NMR spectrometer, for catalysts dispersed in D_2O, and with calibration against tetramethylsilane.

Results and Discussion

The time course of hydrogen evolution from a UV-irradiated TBA$[Ca_2Nb_3O_{10}]$ sample suspended in aqueous methanol or water is shown in Figure 2A (values given in Table 1). In methanol solution, steady evolution of H_2 takes place over 72 h at nearly constant rate. If TBA$[Ca_2Nb_3O_{10}]$ is irradiated in water, substantially less H_2 is formed, and after 48 h the H_2 rate begins to drop to 20% of the initial rate. For TBA$[Ca_2Nb_3O_{10}]$ modified with 3 wt % Pt particles, the H_2 rate from water diminishes after 9 h of irradiation.[29] However, evacuating the atmosphere above the solution and then flushing with Ar gas temporarily restores the H_2 evolution rate to 60% of the original activity, as shown in Figure 2B.

TABLE 1: H_2 Evolution Data

	nanosheets in H_2O		nanosheets in 20% MeOH	
initial pH	8.3		10.6	
irradiation time	0−48 h	48−78 h	0−48 h	48−78 h
H_2 (μmol)	76.2	9.26	379.8	227.7
H_2 rate (μmol/h)	1.59	0.31	7.91	7.59
QE (%)	0.15	0.03	0.76	0.73

Considering previous work for TiO_2,[9−11,18−20] we suspected that deactivation of the catalyst occurred because of the accumulation of hydrogen peroxide on the catalyst surface. To determine any peroxides formed in the reaction, nanosheets were titrated with the redox indicator *o*-tolidine in the presence of colloidal Pt as a catalyst, as described previously.[11,18,20] The reaction at pH > 3 initially leads to a quinone−diimine complex (Supporting Information) with an absorbance maximum at 625 nm corresponding to a blue color. When *o*-tolidine is added to a suspension of catalyst (pH = 10.5) that had been irradiated for 6 h, this blue color develops within 30 s. Nonirradiated samples do not show the blue color, and neither does the supernatant of irradiated samples after removal of the catalyst. This shows that the H_2O_2 is generated photochemically and that it is associated with the catalyst. After acidification of the solution to pH < 3, the amount of peroxide can be quantified using the 438 nm absorbance of the free diimine (Figure 3 and Table 2). It can be seen that the intensity of the absorbance peak increases with extended irradiation periods as more peroxide was generated. After 6 h of irradiation, one determines a value of 8.97 ± 1.24 μmol, and after 24 h this amount increases to 30.46 ± 3.40 μmol. Nonirradiated nanosheet samples were also tested and possessed a weak absorbance at 438 nm, which should be attributed to trace amounts of peroxide developed during sample storage.

Evolution of H_2 in the gas phase was measured concurrently with peroxide titration. After 6, 12, or 24 h of irradiation, a near 1:1 stoichiometric H_2:H_2O_2 ratio is observed, in agreement with the electron balance of the reaction. This establishes reaction 2 as the net catalytic process in water.

IR and Raman spectroscopy were employed to further characterize the photogenerated peroxide (Figure 4 and Table 3). Peaks at 580, 778, and 940 cm^{-1} in the IR spectrum and their counterparts in the Raman spectrum were present on

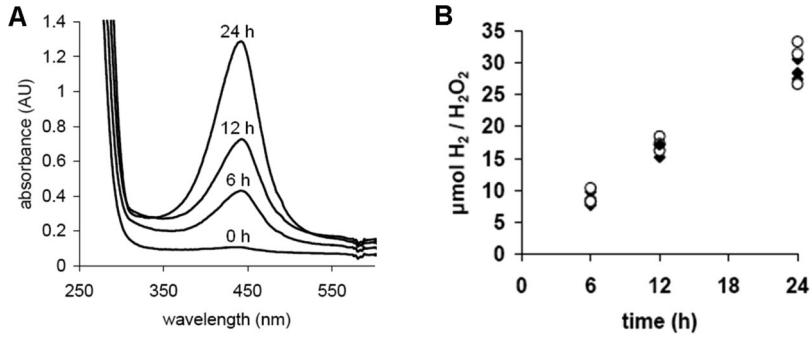

Figure 3. (A) UV−vis absorption spectra showing absorbance at 438 nm of the protonated diimine as irradiation times were increased. (B) Time-resolved H_2 (●) and H_2O_2 (○) evolution data.

TABLE 2: H_2 / H_2O_2 Stoichiometry[a]

irradiation time (h)	H_2 (μmol)	H_2O_2 (μmol)	ratio H_2:H_2O_2
6	8.76 ± 1.04	8.97 ± 1.24	1:0.98
12	16.22 ± 1.39	17.70 ± 1.13	1:0.92
24	28.81 ± 1.59	30.46 ± 3.40	1:0.94

[a] All values are based on three separate measurements for each irradiation time.

nanosheets recovered from both irradiated and nonirradiated samples. Based on a comparison with $KCa_2Nb_3O_{10}$, and $HCa_2Nb_3O_{10}$ (Figure 4A), the bands at 940 and 778 cm^{-1} were assigned to Nb═O and Nb−OH on the sheet surface. As surface sites, these bonds are expected to react most sensitively to cation exchange and protonation.

The band at 580 cm^{-1} was assigned to Nb−μ_2-O bonds within the sheets.[36,37] This represents the majority of Nb−O bonds in the material, giving this absorption the strongest intensity in the spectrum. The broadness of this peak results from inequivalency of the Nb−O bonds that belong to surface and buried Nb-μ_2-O sites (Figure 1C). After irradiation, new peaks at 423, 482, and 873 cm^{-1} appeared in the IR spectrum and a set of corresponding peaks in the Raman spectrum (black traces in Figure 4B, C). The band at 873 cm^{-1} was assigned to ν[O−O] stretching of a peroxo group, which is generally found in the 850 − 910 cm^{-1} range when bound to metal ions.[38−40] The peak at 482 cm^{-1} can be attributed to an asymmetric ν_a[Nb(O_2)] stretch of the peroxo group, given its relative weakness when compared to the strong corresponding peak at 481 cm^{-1} in the Raman spectrum. Thus, the peak at 423 cm^{-1} in the IR spectrum is likely a symmetric ν_s[Nb(O_2)] stretch. Symmetric and asymmetric ν[Nb(O_2)] stretches are generally found to absorb in the range of 430−520 cm^{-1}.[38,40]

In order to verify these assignments, we also prepared peroxide-coated nanosheets by direct reaction of TBA-[$Ca_2Nb_3O_{10}$] with 0.2 M H_2O_2. The peroxide derivative begins to precipitate from such a mixture after 3 h. It can be seen that the vibrational spectra recorded for this material (red traces in Figure 4B, C) are very similar to those obtained for the irradiated nanosheets. However, all new peak bands are stronger than for the irradiated sample, suggesting that the peroxide concentration on the nanosheets is higher. Also noticeable now is a small blue shift of the Nb−OH and Nb−μ_2-O bands by ∼15 cm^{-1}, exposing a shoulder in the Nb−μ_2-O band at 557 cm^{-1}. While both Nb═O and Nb−OH bands are weakened in the IR, the Raman shows the Nb−OH band at nearly unchanged intensity. The selective weakening of the Nb═O band indicates that the H_2O_2 selectively coordinates to the former Nb═O sites.

Most of the spectral changes caused by H_2O_2 coordination can be reversed upon heating the treated nanosheets to 450 °C. IR spectra shown in Figure 4D reveal a disappearing ν(O−O) band at 873 cm^{-1} as the temperature is increased. The ν(Nb═O) band, which had disappeared upon treatment with H_2O_2, reappears, and concurrently the ν(Nb−OH) band shifts back to its original position of 778 cm^{-1}. The ν(Nb−μ_2-O) band at 589 cm^{-1} (not shown) and the Nb═O band at 928 cm^{-1} appear slightly shifted from their original positions. This indicates that while most of the surface-bound peroxide is thermally decomposed and replaced by Nb═O bonds, some distortion remains that shifts these bands. The high stability of peroxide seems to be the primary reason for the inability of the niobate nanosheets to catalyze the overall water splitting reaction (eq 1).

To elucidate the origin of the coordinated peroxide and to confirm peak assignments, we also performed a series of experiments in >98% $H_2{}^{18}O$ water. IR and Raman spectra for TBA[$Ca_2Nb_3O_{10}$] that had been stored in ^{18}O water for 1 week and then irradiated for 20 h are shown in Figure 4B, C (blue trace). The IR spectrum shows a reduction of the Nb−OH and Nb═O bands, and the appearance of a broad peak at 879 cm^{-1} belonging to the ν(O−O) mode. The peak is broadened because partial isotopic substitution produces three independent species $^{18}O-{}^{18}O$, $^{18}O-{}^{16}O$, and $^{16}O-{}^{16}O$, with deviating absorption bands (823, 848, and 873 cm^{-1}, respectively) in this area. Accordingly, the Raman spectrum also shows a broad O−O band at 890−840 cm^{-1}, and two broadened bands at 433 and 473 cm^{-1} for the symmetric and asymmetric ν_a[Nb($^{18/16}O_2$)] stretching vibrations of a side-on coordinated peroxide.

If the nanosheets are kept in $H_2{}^{18}O$ for 1 week, but not irradiated, the ν_a[Nb($^{18/16}O_2$)] bands are absent in the Raman spectrum (green trace in Figure 4B). However, the broad band at 890−840 cm^{-1} remains, which we attribute to contamination of the recycled $H_2{}^{18}O$ with peroxide from previous experiments. Simple storage of the nanosheets in $H_2{}^{18}O$ also causes the Nb−μ_2-O bands to shift to lower wavenumbers, indicating isotopic exchange of even the bridging ^{16}O ions with ^{18}O. Thermal isotope exchange of terminal and bridging O has been previously observed for the Lindqvist cluster ion $[Nb_6O_{16}]^{6-}$, which contains 1 μ_6-O, 6 terminal O, and 12 μ_2-O sites.[41] In this case, room-temperature ^{17}O-nuclear magnetic resonance reveals that the terminal and the μ_2-oxygen ions can be exchanged over the course of hours to days, with rates strongly dependent on pH.

There are several possibilities for H_2O_2 to bind to the nanosheets (Figure 1D), including end-on, η^2, or $\mu_2-\eta^1$-bridging modes. A $\mu_2-\eta^2$ mode, in which one O_2^{2-} ion connects two adjacent metal ions, has been suggested for TiO_2,[18] but is impossible for $HCa_2Nb_3O_{10}$ due to the larger Nb−Nb separation on the nanosheet surface. Side-on coordinated O_2^{2-} is frequently observed in molecular Nb(5+) complexes, including $[Nb(O_2)F_5]^{2-}$,[42] [Nb(O_2)$_3$(phen)],[43] and [Nb(O_2)$_2$(tart)] (tart = tartrate)[44] which

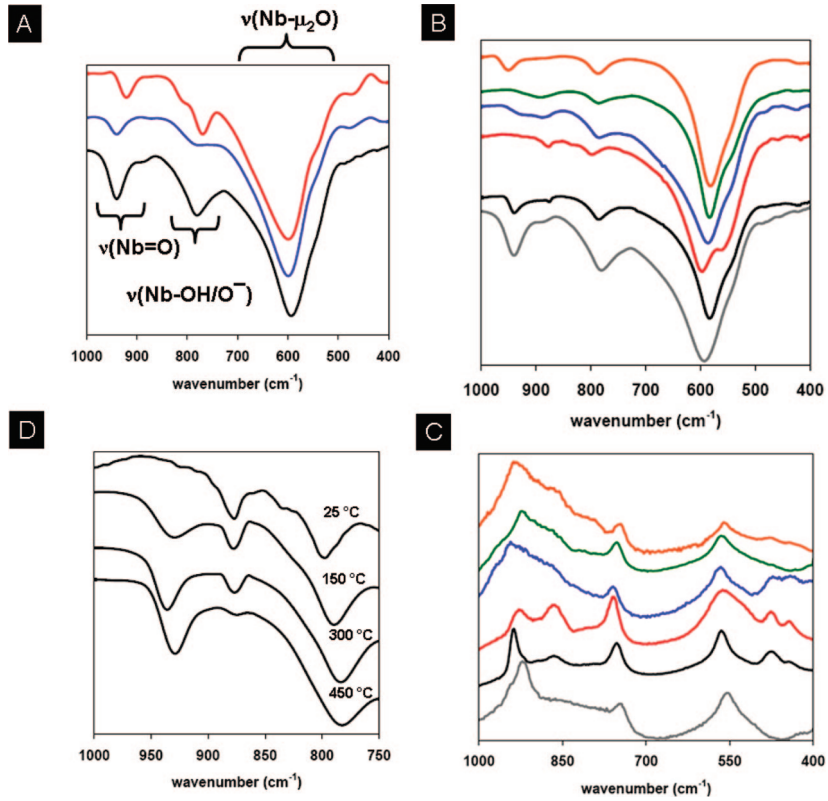

Figure 4. (A) Infrared spectra of $KCa_2Nb_3O_{10}$ (top), $HCa_2Nb_3O_{10}$ (middle), and $TBACa_2Nb_3O_{10}$ (bottom). (B) IR and (C) Raman spectra of $TBACa_2Nb_3O_{10}$ before (gray) and after (black) irradiation in H_2O, after storage (green) and irradiation (blue) in $H_2{}^{18}O$, after treatment with H_2O_2 (red), and after irradiation in air (orange). (D) IR showing thermal removal of H_2O_2.

TABLE 3: IR and Raman Vibrational Data[a]

	ν(Nb═O)		ν(Nb−OH)		ν(Nb−O)		ν(O−O)		ν_a[Nb(O$_2$)]		ν_s[Nb(O$_2$)]	
	IR	Raman	IR	Raman	IR	Raman	IR	Raman	IR	Raman	IR	Raman
irr.	940	939	778	758	580	571	873	870	482	481	423	441
nonirr.	939	925	779	751	578	561	—	—	—	—	—	—
react. with H_2O_2	—	934	793	762	594 557	566	872	871	458	481	418	448

[a] Repeated collection of spectra showed variance in the location of Raman peaks ±8 cm^{-1}, while IR peaks varied ±3 cm^{-1}.

feature up to three peroxide ligands and seven/eight coordinate Nb ions*. For $HCa_2Nb_3O_{10}$, the vibrational spectra discussed above favor the Nb−η^2-O_2 mode, because it is the only mode that gives rise to the asymmetrical and symmetrical ν[Nb(O$_2$)] bands observed around 420−480 cm^{-1}. Also, only this mode gives a nonpolar O−O bond, which is weakly IR-active and strongly Raman-active, as observed in Figure 4B, C (red traces). Based on the relative signal intensities of the Nb═O and Nb−OH Raman bands after irradiation or treatment with H_2O_2 (gray, black, red traces in Figure 4C), there seems to be a preference for the peroxide ions to coordinate to Nb ions of the Nb═O sites. This ligand substitution could occur without disturbing the charge balance of the Nb═O group and could be thought of as a thermodynamically controlled acid−base equilibrium in which the more acidic H_2O_2 ($pK_A = 11.6$) displaces the less acidic water ($pK_A = 15.7$) from its salt. By contrast, incorporation of the peroxide at the Nb−OH sites would lead to a buildup of negative charge or produce a terminal Nb-OOH, which is not observed in the IR. The increase of the coordination number of the Nb−η^2-O_2 sites from six to seven should cause a local distortion of the resulting Nb(μ_2-O)$_6$(O$_2$) polyhedron and adjacent NbO_6 octahedra. This might explain the observed shift of the Nb−μ_2-O stretching bands to higher energy in irradiated or H_2O_2-treated nanosheets.

There are two possible routes for the formation of side-on bonded peroxide in this system, either by two-electron oxidation of water (eq 2) or by two-electron reduction of small traces of O_2 (eq 3). To distinguish among these pathways, we conducted O_2 uptake experiments with the irradiated catalysts in the presence of O_2 and analyzed reaction products with vibrational spectroscopy, NMR, and titrations with the redox indicator. The results of the O_2 uptake experiment are presented in Figure 2C. Only minor O_2 uptake (~1 μmol of O_2) occurred when the catalyst dispersion was stirred in the dark for 18 h, which should be attributed to dissolution of the gas in the water. Upon irradiation, O_2 was removed from the atmosphere at an average rate of 6.3 μmol/h for the first 10 h. This rate slowed from that point to 3.6 μmol/h until all O_2 was removed from the system after 18 h of irradiation. During O_2 adsorption, only 2.52 μmol of H_2 was evolved over 30 h of irradiation, giving a rate of 0.084 μmol/h. This rate is more than 20 times lower than what is observed in the absence of added O_2.[31] About 6.22 μmol of peroxide was detected in the supernatant by *o*-tolidine titration, but only amounts comparable to nonirradiated nanosheets were found associated with the catalyst. When the catalyst suspension was irradiated in air, weak peroxide bands could also be observed in the vibrational spectra (Figure 4B, C, orange traces).

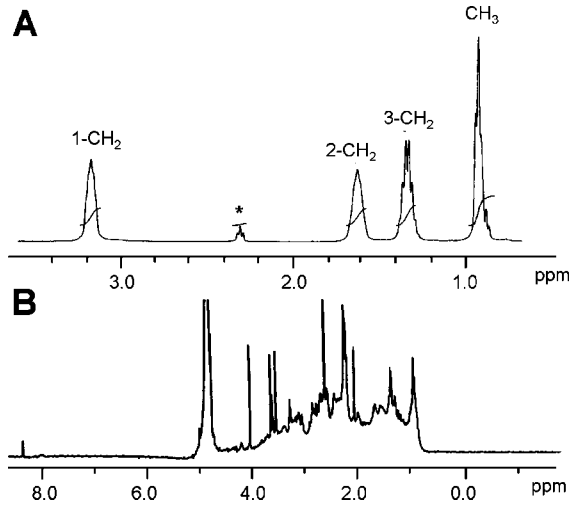

Figure 5. ^{1}H-NMR spectra (300 MHz, D_2O) of residue from irradiated $TBACa_2Nb_3O_{10}$ suspension: (A) after irradiation in Ar atmosphere and (B) after irradiation in air atmosphere. * indicates impurity.

^{1}H-NMR spectra collected for the catalyst suspension after irradiation in argon or air atmosphere are shown in Figure 5. Irradiation in the absence of O_2 does reveal peaks for the TBA counterion, with only minor downfield shift (+0.1 ppm) compared to a nonirradiated catalyst (spectrum not shown). Samples irradiated in air show a drastically changed spectrum with broad peaks at 4.194−0.908 ppm and a weak peak at 8.338 ppm, which could be indicative of an amide species. Only traces of the original TBA^+ are preserved, suggesting partial decomposition of the tetrabutylammonium cation under these conditions. This decomposition of the counterion is also supported by the observation that the catalyst precipitates when the irradiation is performed in air, whereas no precipitation occurs in argon atmosphere. TBA decomposition can be explained by assuming that irradiation in air produces superoxide radicals via one-electron reduction of O_2 (eq 4) which react with TBA under H abstraction and H_2O_2 formation (eq 7). These reactions are known to be involved in the photochemical remediation of organic waste.[45−49] Most of the H_2O_2 formed in this way would not be associated with the catalyst, while some of it could adsorb to the niobate sheets by direct reaction, as described above. Conversely, irradiation in the absence of air produces side-on coordinated peroxide by two-electron oxidation of water (eq 2), without free radical intermediates.

Conclusion

The principle conclusions from this work are the following:

1. Niobate nanosheets photocatalytically decompose water stoichiometrically into H_2 and H_2O_2.

2. The peroxide coordinates as a side-on ligand to the surface Nb(5+) ions but can be removed by heating the solid catalyst to 450 °C, or, partially, by purging of the catalyst dispersion with Ar in solution. The high stability of the Nb−peroxide bond seems to be the reason for the inability of the nanosheets to evolve O_2 under irradiation with UV light.

3. Based on $H_2{}^{18}O$ studies the peroxide forms by two-electron oxidation of water (eq 6) or by direct reaction of the niobate with H_2O_2. The photochemical formation of the peroxide does not seem to involve free radicals, based on the integrity of the TBA counterion.

4. Reaction of the niobate nanosheets with $H_2{}^{18}O$ at room temperature leads to isotopic exchange of all O atoms in the nanosheets over the course of 24 h.

5. Irradiation of the catalyst in the presence of air produces free H_2O_2 via reduction of O_2 (eq 4). The decomposition of the tetrabutylammonium counterion indicates that free radicals, e.g., superoxide, are involved in this process (eq 7).

Acknowledgment. This work was supported by an Energy Innovation Startup Grant of the California Energy Commission. We thank Alan Hicklin for help with collecting Raman spectra and NEAT ORU for the use of their facilities. We also thank W. R. Griswald VI for collecting NMR spectra.

Note Added in Proof. The newly discovered cluster ion $[H_3Nb_6O_{13}(O(I)_2)_6]^{8-}$ contains six side-on bonded peroxide ligands. Ohlin, C. A.; Villa, E. M.; Fettinger, J. C.; Casey, W. H. *Angew. Chem. Int. Ed. Engl.* **2008**, *47* (43), 8251–8254.

Supporting Information Available: Details of the reaction of *o*-tolidine with peroxide. This material is available free of charge via the Internet at http://pubs.acs.org.

References and Notes

(1) Fujishima, A.; Honda, K. *Bull. Chem. Soc. Jpn.* **1971**, *44*, 1148.
(2) Fujishima, A.; Honda, K. *Nature* **1972**, *238*, 37.
(3) Maeda, K.; Domen, K. *J. Phys. Chem. C* **2007**, *111*, 7851.
(4) Kamat, P. V. *J. Phys. Chem. C* **2007**, *111*, 2834.
(5) Osterloh, F. E. *Chem. Mater.* **2008**, *20*, 35.
(6) Maeda, K.; Takata, T.; Hara, M.; Saito, N.; Inoue, Y.; Kobayashi, H.; Domen, K. *J. Am. Chem. Soc.* **2005**, *127* (23), 8286–8287.
(7) Maeda, K.; Teramura, K.; Saito, N.; Inoue, Y.; Kobayashi, H.; Domen, K. *Pure Appl. Chem.* **2006**, *78* (12), 2267–2276.
(8) Mills, A.; Porter, G. *J. Chem. Soc., Faraday Trans. 1* **1982**, *78*, 3659.
(9) Yesodharan, E.; Yesodharan, S.; Graetzel, M. *Sol. Energy Mater.* **1984**, *10*, 287.
(10) Kiwi, J.; Grätzel, M. *J. Phys. Chem.* **1984**, *88*, 1302.
(11) Duonghong, D.; Grätzel, M. *J. Chem. Soc., Chem. Commun.* **1984**, 1597.
(12) Ebina, Y.; Sakai, N.; Sasaki, T. *J. Phys. Chem. B* **2005**, *109*, 17212.
(13) Kudo, A.; Kato, H.; Nakagawa, S. *J. Phys. Chem. B* **2000**, *104*, 571.
(14) Tabata, S.; Ohnishi, H.; Yagasaki, E.; Ippommatsu, M.; Domen, K. *Catal. Lett.* **1994**, *28*, 417.
(15) Sayama, K.; Arakawa, H. *J. Chem. Soc., Chem. Commun.* **1992**, 150.
(16) Sayama, K.; Arakawa, H. *J. Photochem. Photobiol., A* **1994**, *77*, 243.
(17) Arakawa, H. Water Photolysis by TiO_2 Particles—Significant Effect of Na_2CO_3 Addition on Water Splitting. In *Photocatalysis Science and Technology*; Kaneko, M., Okura, I., Eds.; Springer: New York, 2002; p 235.
(18) Kiwi, J.; Graetzel, M. *J. Mol. Catal.* **1987**, *39*, 63.
(19) Kalyanasundaram, K.; Grätzel, M.; Pelizzetti, E. *Coord. Chem. Rev.* **1986**, *69*, 57.
(20) Gu, B.; Kiwi, J.; Grätzel, M. *New J. Chem.* **1985**, *9*, 539.
(21) Goto, H.; Hanada, Y.; Ohno, T.; Matsumura, M. *J. Catal.* **2004**, *225*, 223.
(22) Augustynski, J. *Electrochim. Acta* **1993**, *38*, 43.
(23) Ulmann, M.; Detacconi, N. R.; Augustynski, J. *J. Phys. Chem.* **1986**, *90*, 6523.
(24) Domen, K.; Yoshimura, J.; Sekine, T.; Tanaka, A.; Onishi, T. *Catal. Lett.* **1990**, *4*, 339.
(25) Ebina, Y.; Tanaka, A.; Kondo, J. N.; Domen, K. *Chem. Mater.* **1996**, *8*, 2534.
(26) Takata, T.; Tanaka, A.; Hara, M.; Kondo, J. N.; Domen, K. *Catal. Today* **1998**, *44*, 17.
(27) Ebina, Y.; Sasaki, T.; Harada, M.; Watanabe, M. *Chem. Mater.* **2002**, *14*, 4390.
(28) Yamashita, Y.; Hyuga, K.; Petrykin, V.; Kakihana, M.; Yoshimura, M.; Domen, K.; Kudo, A. *J. Ceram. Soc. Jpn.* **2007**, *115*, 511.
(29) Compton, O. C.; Mullet, C. H.; Chiang, S.; Osterloh, F. E. *J. Phys. Chem. C* **2008**, *112*, 6202.
(30) Carroll, E. C.; Compton, O. C.; Madsen, D.; Larsen, D. S.; Osterloh, F. E. *J. Phys. Chem. C* **2008**, *112*, 2394.
(31) Compton, O. C.; Carroll, E. C.; Kim, J. Y.; Larsen, D. S.; Osterloh, F. E. *J. Phys. Chem. C* **2007**, *111*, 14589.
(32) Proper, R.; Rosenthal, R. W. *Chem. Anal.* **1956**, *45*, 79.

(33) Jacobsen, A. J.; Johnson, J. W.; Lewandowski, J. T. *Inorg. Chem.* **1985**, *24*, 3727.

(34) Fang, M. M.; Kim, C. H.; Saupe, G. B.; Kim, H. N.; Waraksa, C. C.; Miwa, T.; Fujishima, A.; Mallouk, T. E. *Chem. Mater.* **1999**, *11*, 1526.

(35) Kuhn, H. J.; Braslavsky, S. E.; Schmidt, R. *Pure Appl. Chem.* **2004**, *76*, 2105.

(36) Pilipenko, A. T.; Shevchenko, L. L.; Patselyuk, V. A. *J. Appl. Spectrosc.* **1970**, *14*, 473.

(37) Andrade, J. S. d.; Pinheiro, A. G.; Vasconcelos, I. F.; Sasaki, J. M.; Paiva, J. A. C. d.; Valente, M. A.; Sombra, A. S. B. *J. Phys.: Condens. Matter* **1999**, *11*, 4451.

(38) Nakamoto, K. *Infrared and Raman Spectra of Inorganic and Coordination Compounds*, 5th ed.; Wiley-Interscience: New York, 1997.

(39) Bayot, D.; Tinant, B.; Devillers, M. *Catal. Today* **2003**, *78*, 439.

(40) Bayot, D.; Devillers, M.; Peeters, D. *Eur. J. Inorg. Chem.* **2005**, *20*, 4118.

(41) Black, J. R.; Nyman, M.; Casey, W. H. *J. Am. Chem. Soc.* **2006**, *128*, 14712.

(42) Stomberg, R. *Acta Chem. Scand. A* **1983**, *37*, 523.

(43) Mathern, G.; Weiss, R. *Acta Crystallogr., Sect. B* **1971**, *B 27*, 1582.

(44) Bayot, D.; Tinant, B.; Devillers, M. *Inorg. Chem.* **2005**, *44*, 1554.

(45) Fox, M. A.; Dulay, M. T. *Chem. Rev.* **1993**, *93*, 341.

(46) Carp, O.; Huisman, C. L.; Reller, A. *Prog. Solid State Chem.* **2004**, *32*, 33.

(47) Halmann, M. M. *Photodegradation of Water Pollutants*; CRC Press: Boca Raton, FL, 1996.

(48) Kamat, P. V. *J. Phys. Chem. B* **2002**, *106*, 7729.

(49) Vinodgopal, K.; Hotchandani, S.; Kamat, P. V. *J. Phys. Chem.* **1993**, *97*, 9040.

JP807839B